Microdisc HgCdTe lasers operating at 22-25 μm under optical pumping

A. A. Razova[1,2,*], V. V. Rumyantsev[1,2], K. A. Mazhukina[1], V. V. Utochkin[1], M. A. Fadeev[1], A. A. Dubinov[1,2], V. Ya. Aleshkin[1,2], N. N. Mikhailov[3], S. A. Dvoretsky[3], D. V. Shengurov[1], N. S. Gusev[1], E. E. Morozova[1], V. I. Gavrilenko[1,2], S. V. Morozov[1,2]

[1]Institute for Physics of Microstructures of Russian Academy of Sciences, Nizhny Novgorod 603950, Russia

[2]Lobachevsky State University, Nizhny Novgorod 603950, Russia

[3]Institute of Semiconductor Physics, Siberian Branch of Russian Academy of Sciences, Novosibirsk 630090, Russia

*e-mail: annara@ipmras.ru

Abstract

Lasing from HgCdTe microdisc cavities is demonstrated at wavelengths as long as 22 — 25 μm. The optical threshold and operation temperature are far from being limited by intrinsic recombination processes. The employed ion etching technology appears to introduce additional defects in the vicinity of the microdiscs, degrading figures of merit as the height of the cavity increases. However, a watt-level mid-infrared pumping source should suffice for lasing in microdiscs with moderate height and ~100 μm diameter.

Keywords: HgCdTe, microdisc cavities, whispering gallery modes, interband laser, ion etching, laser lithography

After more than 60 years of intense development compact semiconductor lasers have become ubiquitous light sources for spectroscopy tasks in both applications and fundamental research. As far as the mid-infrared (IR) range is concerned, quantum cascade lasers (QCLs) approach their 30-year-anniversary with excellent figures of merit. However, currently there still is the "terahertz gap" located in the wavelength range of 25 – 60 μm, where QCLs face formidable difficulties. For QCL based on A3B5 semiconductors, wavelengths from 30 to 55 μm feature strong phonon absorption. At the moment only a few QCLs are able to lase at individual wavelengths in 25-28 μm region [1, 2, 3], while the rest of the "terahertz gap" remains inaccessible.

It has been proposed to use alternative materials to bridge this gap. Terashima and Hirayama [4] employed GaN for the active region of the QCL, which allowed generation at wavelengths of 54.8 μm and 43 μm at temperatures around 5 K. Using a combination of GaAs/AlGaAs materials, Shahili et al [5] were able to obtain not only pulsed operation, but also a continuous wave regime in the wavelength range of 50 – 63 μm for cryogenic temperatures. However, there is still a strong absorption region in these and similar materials, which does not allow the "terahertz gap" to be completely covered. In addition, suitable substrates are scarce for a number of alternative materials, in particular GaN.

On the other hand, interband lasers based on narrow-gap materials can deliver radiation sources in the range of 25 – 60 μm, for which the main non–radiative process, Auger recombination, is suppressed due to a peculiar carrier dispersion [6]. Narrow-gap alloys of lead-tin chalcogenides have a hyperbolic carrier dispersion law. It is known that in this case threshold Auger recombination is prohibited, since it is impossible to fulfill the laws of energy-momentum conservation. This fundamental effect, as well as the possibility of varying the bandgap in a wide spectral range, makes it possible to obtain radiation in the long-wavelength region of the mid-IR range in the interband lasers based on PbSnTe and PbSnSe. The latest attempt achieved generation at a wavelength of 50.4 μm [7]. However, the operating temperature of such lasers did not exceed the temperature of liquid nitrogen. A further increase in the operating temperature and generation wavelength is limited by technological difficulties, one of which is the large residual concentration of carriers (typically not less than 10^{17} cm^{-3}).

Heterostructures with quantum wells (QW) based on another narrow-gap alloy – HgCdTe – also provide a hyperbolic law of carrier dispersion in the vicinity of $k = 0$ [8], allowing

suppression of the threshold-type Auger recombination. The value of the minimum kinetic (threshold) energy sufficient for Auger process strongly depends on the composition and thickness of the QW. The threshold value follows the position of the side maxima of the first valence band: the lower the energy of the side maxima, the higher the threshold energy of the Auger process. By optimizing the parameters of the structures, we have recently demonstrated stimulated emission (SE) in the IR-range up to 31 μm [9]. It is also known that optical phonons in HgCdTe alloys entail *Reststrahlen* bands in the region of 60 – 80 μm [10]. Therefore, heterostructures with HgCdTe/CdHgTe QW are a promising material for interband lasers operating in the "terahertz gap" region [11, 12].

Though a number of works focus on HgTe quantum dots [13, 14, 15], studies of light emission from HgCdTe-based QWs were limited to photoluminescence (PL) and SE as far as wavelengths above 10 μm are concerned. Forming a resonant cavity by cleaving is complicated for a vicinal substrate orientation, like (013) or (211), which is typical for epitaxial HgCdTe. In recent works, photolithography and ion etching were successfully employed to produce both stripe [16] and microdisc cavities for mid-IR emitters. In microdisc lasers with thin HgCdTe QWs, laser action was demonstrated in the 3 – 5 μm atmospheric transparency window at temperatures achievable with thermoelectric cooling [17]. However, in works [16, 17] the etching depth was large enough so that QWs in the active region were prone to defect formation on the cavity walls.

In this article, we focus on microdisc cavities with HgCdTe/CdHgTe QWs designed to operate in the wavelength range of 20 – 25 μm. By implementing metal masks and explosive lithography we vary the microdisc height and analyze the performance of the lasers. The results show that laser emission (LE) is possible for moderate etching depths despite a considerable damage introduced by ion etching.

Structure under study contained N = 20 $Hg_{1-x}Cd_xTe/Cd_yHg_{1-y}Te$ QWs with x=0.026, y=0.62 and thicknesses of 5.4 nm. The structure was grown by molecular beam epitaxy (MBE) on a *n*++-GaAs(013) substrate (Fig. 1a). Heavily doped substrate allows one to minimize the ratio of the mode losses (α) to the optical confinement factor (Γ-factor) in relatively thin waveguide layers [18].

Single microdisc cavities with diameters of 200 μm were formed by etching with argon ions. Long operating wavelengths imply thick waveguides and therefore the etching selectivity may not be high enough to achieve desirable etching depth when using a photoresist mask. To increase the attainable etching depth a metal mask was deposited by the explosive lithography before the etching process. The metal mask was also expected to improve the verticality of cavity walls and thus reduce the associated radiation output losses if any.

Etching was carried out at three characteristic depths: 3.4 μm (microdisc #1201d), 4.3 μm (microdisc #1201c), 8 μm (microdisc #1201a) (Table 1). Accordingly, outside the disk area the etching removed 1) the cover layer and partially the upper waveguide layer, 2) the cover layer, the upper waveguide layer and a part of the active region, 3) the cover layer, the upper waveguide layer, the QW array and partially the lower waveguide layer (Fig. 1 e-g). The height of the microdiscs was determined using a scanning electron microscope (SEM) (Fig. 2).

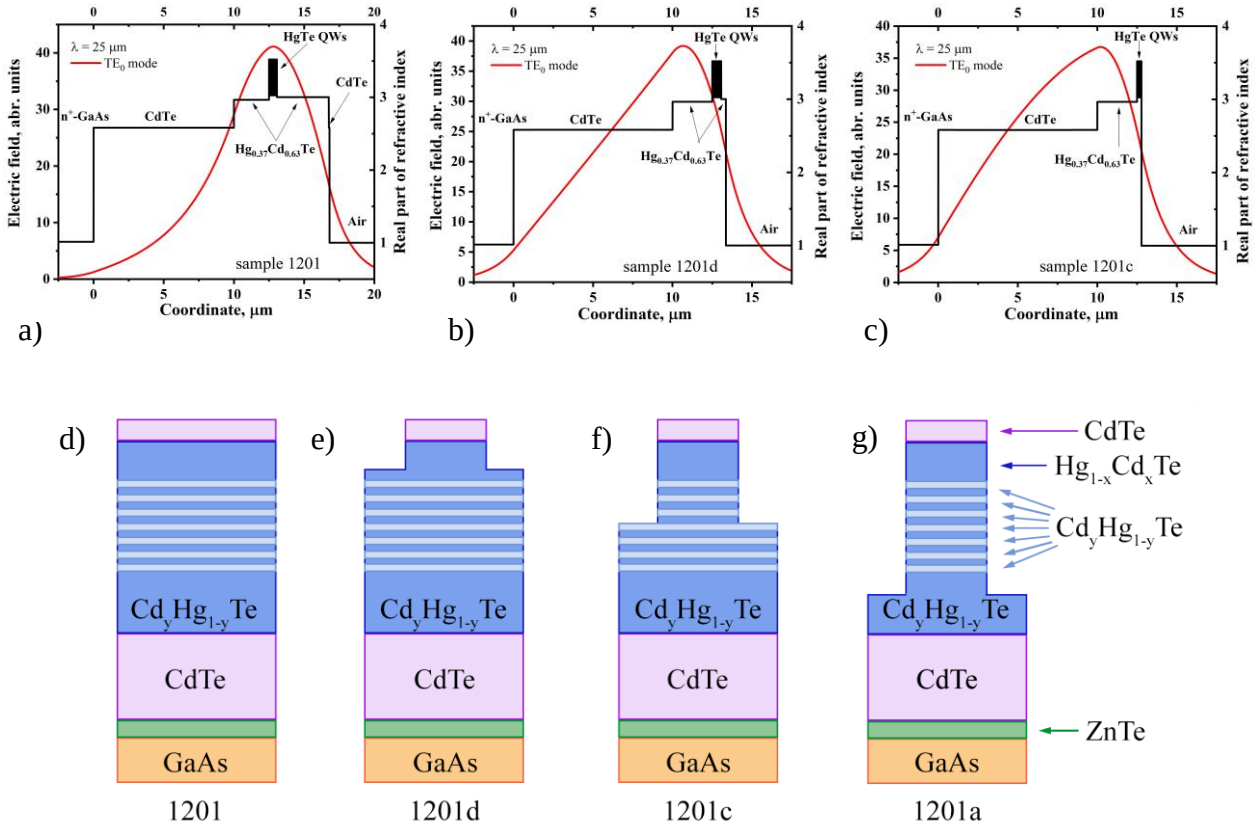

Fig. 1. Calculated optical confinement in samples after a) no etching (sample #1201, scheme at part (d)); b) etching to a depth of 3.4 μm (sample #1201d, scheme at part (e)); c) etching at 4.3 μm (sample #1201c, scheme at part (f)). The black line shows the real part of the refractive index of the layers, the red line shows the calculated distribution of the TE_0-mode field in the structure

under study for a wavelength of 25 μm. Parts (d)-(g) illustrate structure layers (not to scale) and the etching depth for different samples under study (Table 1).

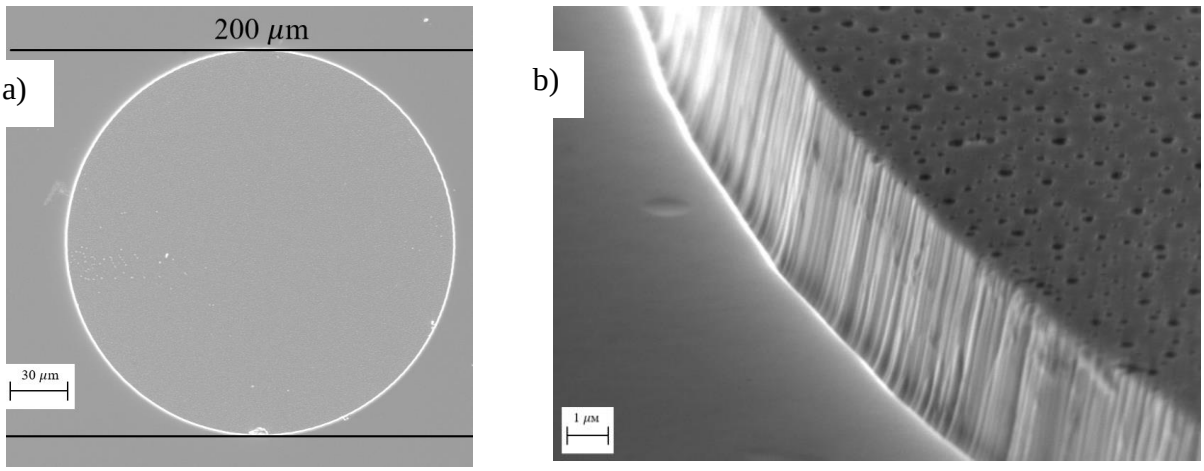

Fig. 2. SEM images of microdisc cavity #1201d (diameter 200 μm): a) top view, b) side view.

To measure the emission spectra, the samples were mounted on a cold plate of a closed-loop optical helium cryostat with the possibility of temperature adjustment from 8 to 300 K. Using an elliptical mirror, the cryostat was optically coupled to one of the inputs of the Bruker Vertex 80v Fourier transform IR spectrometer. The measurements were carried out in the step scan mode [19], allowing us to use a pulsed CO_2 laser for pumping. The pumping radiation was incident normally at the surface of the sample, and the radiation from the sample was collected at an angle of 2-5° relative to the surface. The pulse duration of the CO_2 laser was ~ 100 ns, and the repetition rate was up to 50 Hz. The maximum energy was ~10 mJ per pulse. HgCdTe photoresistor (with a 24 μm cutoff) and a silicon bolometer were used as detectors.

Table 1. The parameters of samples under study: L – the depth of the upper QW; l – the depth of the lower QW; P_{th} – the threshold pumping power density at 35 K for SE or LE; τ – effective carrier lifetimes at 35 K estimated from SE/LE thresholds**,** T_{max} – the maximum observation temperature of SE or LE.

Sample	Etching depth, μm	L/l, μm	α/Γ, cm^{-1}	$P_{th(SE)}$, kW/cm^2	$P_{th(LE)}$, kW/cm^2	τ, ps	$T_{max(SE)}$, K	$T_{max(LE)}$, K

#1201	0	3.85/4.6	18	0.5±0.2	---	150	95±2	---
microdisc #1201d	3.4	3.85/4.6	250	7.5±1	12±1	8/5	75±2	60±2
microdisc #1201c	4.3	3.85/4.6	1466	9±1	35±3	8/1.7	50±2	50±2
Microdisc #1201a	8	3.85/4.6	---	---	---	---	---	---

As mentioned above, the microdiscs were processed from the HgCdTe heterostructure grown on a doped GaAs substrate. The concentration of free carriers in the substrate was ~ 10^{18} cm^{-3}. Such n^{++}-GaAs substrate has a high reflection coefficient in the long-wavelength range, which is why even when the upper waveguide layer is removed (Fig. 1e,f) the TE_0 mode is still localized in the waveguide (Fig. 1b,c). As a result, by varying the pumping beam diameter with a diaphragm we were able to switch between the spectrum dominated by the microdisc emission to the one dominated by SE in a waveguide TE_0 mode (when the entire surface of the structure was optically pumped). Such approach facilitated the analysis of the experimental data by comparing the figures of the merit for emission from the microdisc cavity and the waveguide.

Resolution of 0.1 cm^{-1} (0.012 meV) allowed us to reveal the mode pattern on the emission spectra of the microdisc cavities (Fig. 3a). The theoretical value of the intermode distance for the whispering gallery modes (WGMs), calculated in the first approximation [20, 21], is 0.62 meV, which is in good agreement with the experimental spectra. At the same time, the modes are observed not of the same radial order, but of different ones with different

azimuthal numbers. Boxcar apodization yields 0.031 meV for the spectral width of the lines at 0.12 meV resolution, while the typical width of the SE spectrum ~ 3 meV [9, 16-17].

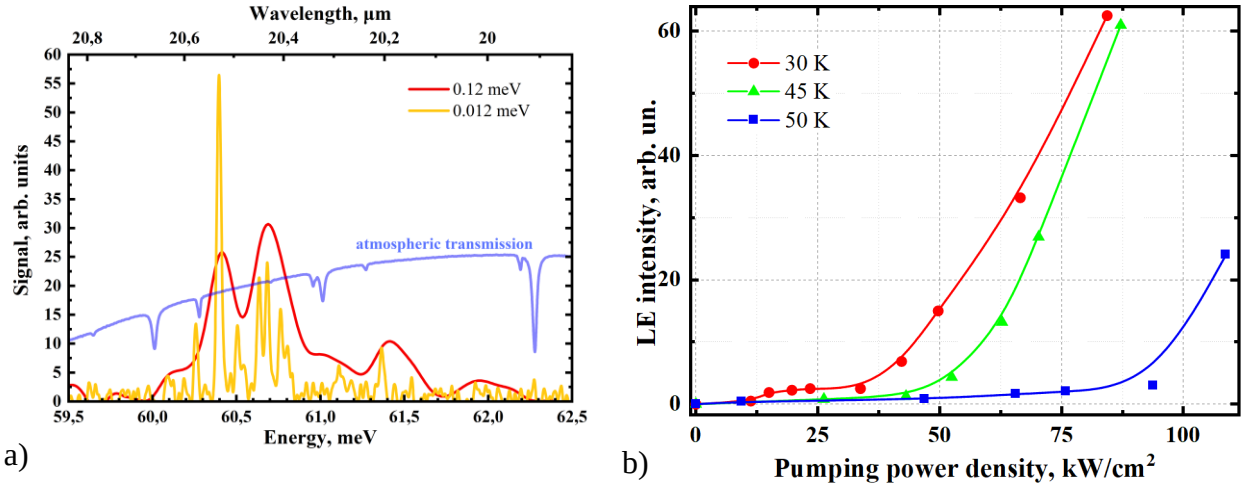

Fig. 3. a) The LE spectra of microdisc #1201c at a temperature of 45 K measured with different resolution (see legend). The transmission spectrum of the atmosphere with a resolution of 0.012 meV is also shown. b) Dependence of the emission signal on the pumping power density for microdisc #1201c at different temperatures.

It can be noted that with an increase in the etching depth, the threshold pumping power density rises and the maximum "operating" temperature drops for both LE and SE in comparison to the SE from the initial structure (Table 1). In accordance with this trend, there is no laser emission from the microdisc with the etching depth of 8 μm (#1201a). The figures of merit can suffer from: (i) defects of the active region, intensifying the Shockley – Read – Hall (SRH) type of recombination and thus degrading carrier lifetimes and population inversion; (ii) additional optical losses introduced by etching. In case of the microdiscs the latter is due to the imperfections of cavity walls, enhancing parasitic light scattering and ultimately leading to radiative losses. For a waveguide layers outside the disc, TE_0 mode leaks into the CdTe buffer as the etching removes the upper cladding layer, increasing the ratio of mode losses to the Γ-factor (Fig. 4).

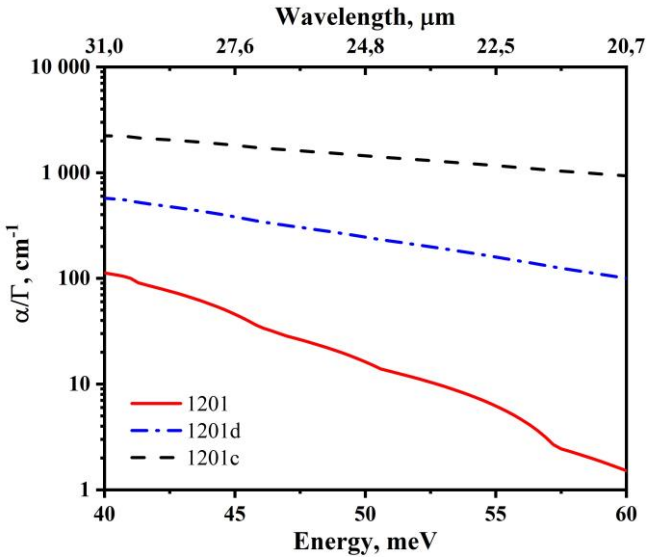

Fig. 4. The dependence of the ratio of mode losses (α) to the optical restriction factor (Γ) on the wavelength (quanta energy) for the samples under study.

Consider the SE from the samples' waveguides at first. The occurrence of additional recombination defects is evident from the dramatic growth of the threshold in the etched samples compared to the initial structure (Table 1). The structure degradation can be described in terms of effective carrier lifetime calculated from the experimental values of the threshold pumping intensity $P_{th(SE)}$ and the calculated gain vs. carrier density curve (Fig. 5). Table 1 gives the corresponding lifetime estimations τ at 35 K. The increase in recombination rates entails drop of the operation temperature $T_{max(SE)}$ as well. Indeed, the threshold concentration of carriers, at which the amplification occurs in the unprocessed structure #1201 at 95 K, is $9 \cdot 10^{10} cm^{-2}$ (Fig. 5). Since the waveguide losses are negligible (Table 1, Fig. 4) and SE at 95 K was observed only at the maximum pumping power of ~ 10^5 kW/cm^2, it can be assumed that such power corresponds to the threshold concentration of carriers at 95 K. When the cover layer and the upper waveguide layer are etched (Fig. 1b,e), the α/Γ ratio in #1201d grows up to 250 cm^{-1} (Table 1, Fig. 4). This value is still low enough to expect the operating temperature around 85 – 90 K (consider Fig. 5) rather than 75 K that is observed in the experiment. In the initial structure, the optical threshold at 75 K is about ~5 kW/cm^2 and carrier lifetimes can be estimated as 44 ps. The lifetime decrease

from 150 ps at 35 K to 44 ps at 75 K results from Auger recombination intensifying with temperature. Carrier lifetimes drop to 8 ps after etching (Table 1) suggest that performance at 77 K can also be considerably compromised by defect-induced recombination, explaining the drop in the operation temperature.

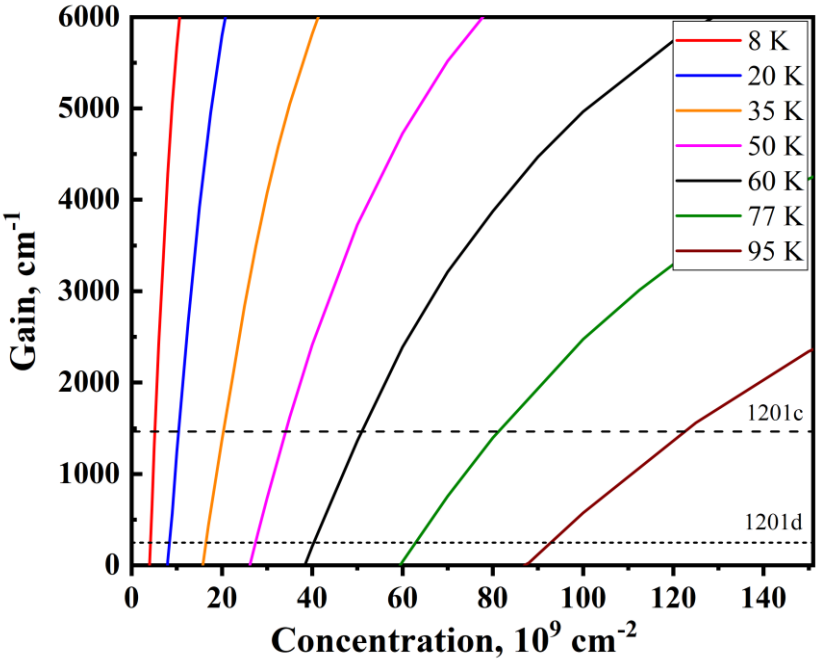

Fig. 5. Material gain vs. non-equilibrium carrier concentration in structure under study at different temperatures.

Nevertheless, further damaging by the ion etching seems to be minor in sample #1201c. The SE threshold at 35 K inches up by a factor of 1.2 compared to #1201d and can be entirely attributed to the increment in the optical losses of the waveguide (Fig. 5). Thus, decrease in operation temperature of SE between 1201*d* and 1201*c* samples should be mainly related to the reduction of Γ-factor in #1201c waveguide (Fig. 4). Similar temperature performance is observed in structures with non-optimized waveguides and wider QWs [22], where carrier lifetimes are degraded not by defect-induced recombination but due to Auger processes.

As for microdiscs, the sharp rise of the threshold (Table 1) indicate either higher defect density in the QWs below the disc or extremely high radiative losses on the cavity walls. The

latter seems to be less plausible because optical losses exceeding that of #1201c waveguide (inferred from higher threshold at 35 K) do not agree well with the temperature performance of the microdiscs. The operation temperature $T_{max(LE)}$ for the microdisc *c* is on par with SE in #1201c, and in microdisc *d* it is even higher, despite that *c* and *d* microdiscs have larger thresholds than SE in #1201c at 35 K. On the contrary, assuming negligible optical losses from the microdiscs one can explain the same quenching temperature for SE and LE in sample #1201c by the fact that less carrier density is needed for the onset of amplification in the cavity.

It may be noted that quantitative agreement with Fig. 5 is quite poor within this interpretation. Namely, the ratio between the threshold intensities of SE and LE in sample #1201c is $R_I = 9/35 = 0.25$ (Table 1), while for the threshold carrier concentrations the ratio at 50 K stands for $R_n = 26/34 = 0.75$ (Fig. 5). This discrepancy most likely stems from carrier heating not taken into account. The heating effects become evident in such structures when pumping intensity exceeds ~10 kW/cm^2 [9]. It therefore follows that the effective carrier temperature is sure to be elevated for microdisc #1201c near the threshold. Thus, the onset of LE actually takes place at higher carrier density than expected from Fig. 5 at 35 K, which means that the degradation of carrier lifetime in Table 1 is overestimated for microdisc #1201c. In addition, the threshold at the quenching temperature is close to the maximum pumping intensity ~ 100 kW/cm^2 and therefore carrier heating may be even stronger. The latter implies that realistic gain vs. carrier density curves grow slower than in Fig. 5. Taking into account both abovementioned factors should improve the agreement between R_I and R_n. For lower pumping intensities, the agreement improves. In microdisc #1201d the threshold carrier density at 60 K corresponds to $3.7 \cdot 10^{10}$ cm^{-2}, which is close to that required for overcoming losses in #1201c waveguide at 50 K ($3.5 \cdot 10^{10}$ cm^{-2}). R_n is thus 37/35 = 1.06. On the other hand, at 35 K the carrier heating is

moderate for a threshold of 12 kW/cm^2 and R_I = 7.5/12 = 0.625 is much closer to R_n for microdisc #1201d.

To conclude, this work demonstrates that microdisc HgCdTe lasers are able to operate at wavelengths as long as 25 μm while previously laser emission for this material was limited to a wavelengths below 5 μm [23, 24]. However, the results reveal a considerable damage induced by the etching, especially in the microdisc area. Better performance was obtained in the mesastructure with lower etching depth so that the etching frontier did not encroach into the active region. Forming such cavities is attainable not only with metal masks but with photoresist as well [16]. Below 35 K, the integral excitation power of several watts would be enough for the onset of interband amplification in the cavities, bringing the QCL-pumped HgCdTe lasers on the verge of feasibility.

The research was carried out within the state assignment of Ministry of Science and Higher Education of the Russian Federation (theme No. 124050300055-9/FFUF-2024-0045).

Conflict of interest: The authors declare that they have no conflict of interest.

References

1. Loghmari, Z., Bahriz, M., Meguekam, A., Teissier, R., Baranov, A. N., "InAs-based quantum cascade lasers emitting close to 25 μm", Electronics Letters **55** (3), 144-146 (2019).

2. Olariu, T., Senica, U., Faist, J., "Single-mode, surface-emitting quantum cascade laser at 26 μm", Appl. Phys. Lett. **124** (4), 041109 (2024).

3. Ohtani, K., Beck, M., Süess, M. J., Faist, J., Andrews, A. M., Zederbauer, T., Detz, H., Schrenk, W., Strasser, G., "Far-infrared quantum cascade lasers operating in the AlAs phonon reststrahlen band", ACS Photonics **3** (12), 2280-2284 (2016).

4. Terashima, W., Hirayama, H., **"**GaN-based terahertz quantum cascade lasers", Proceedings Terahertz Physics, Devices, and Systems IX: Advanced Applications in Industry and Defense **9483**, 948304 (2015).

5. Shahili, M., Addamane, S. J., Kim, A. D., Curwen, C. A., Kawamura, J. H., Williams, B. S., "Continuous-wave GaAs/AlGaAs quantum cascade laser at 5.7 THz", Nanophotonics **13** (10), 1735-1743 (2024).

6. Dimmock, J. O., Melngailis, I., Strauss, A. J., "Band structure and laser action in $Pb_xSn_{1-x}Te$", Physical Review Letters **16** (26), 1193-1196 (1966).

7. Maremyanin, K. V., Ikonnikov, A. V., Bovkun, L. S., Rumyantsev, V. V., Chizhevskii, E. G., Zasavitskii, I. I., Gavrilenko, V. I., "Terahertz Injection Lasers Based on a PbSnSe Solid Solution with an Emission Wavelength up to 50 μm and Their Application in the Magnetospectroscopy of Semiconductors", Semiconductors **52** (12), 1590-1594 (2018).

8. Bernevig, B. A., Hughes, T. L., Zhang, S. C., "Quantum spin Hall effect and topological phase transition in HgTe quantum wells", Science **314** (5806), 1757-1761 (2006).

9. Rumyantsev, V. V., Dubinov, A. A., Utochkin, V. V., Fadeev, M. A., Aleshkin, V. Ya., Razova, A. A., Mikhailov, N. N., Dvoretsky, S. A., Gavrilenko, V. I., Morozov, S. V., "Stimulated emission in 24–31 μm range and «Reststrahlen» waveguide in HgCdTe structures grown on GaAs", Applied Physics Letters **121** (18), 182103-1-182103-5 (2022).

10. Talwar, D. N., Vandevyver, M., "Vibrational properties of HgCdTe system", Journal of Applied Physics **56** (6), 1601-1607 (1984).

11. Menon, V. M., Ram-Mohan, L. R., Vurgaftman, I., Meyer, J. R., “TE- and TM-polarized optoelectronic properties of HgCdTe quantum wells”, Journal of Electronic Materials **29** (6), 865-868 (2000).

12. Alymov, G., Rumyantsev, V., Morozov, S., Gavrilenko, V., Aleshkin, V., Svintsov, D., “Fundamental Limits to Far-Infrared Lasing in Auger-Suppressed HgCdTe Quantum Wells”, ACS Photonics **7** (1), 98-104 (2020).

13. Apretna, T., Nilforoushan, N., Tignon, J., Dhillon, S., Carosella, F., Ferreira, R., Lhuillier, E., Mangeney, J., “Coherent THz wave emission from HgTe quantum dots”, Applied Physics Letters **121** (25), 251101 (2022).

14. Gréboval, C., Chu, A., Goubet, N., Livache, C., Ithurria, S., Lhuillier, E., “Mercury chalcogenide quantum dots: material perspective for device integration”, Chemical Reviews **121** (7), 3627 (2021).

15. Geiregat, P., Houtepen, A. J., Sagar, L. K., Infante, I., Zapata, F., Grigel. V., Allan, G., Delerue, C., Van Thourhout, D., Hens, Z., “Continuous-wave infrared optical gain and amplified spontaneous emission at ultralow threshold by colloidal HgTe quantum dots”, Nature Materials **17** (1), 35 (2017).

16. Utochkin, V., Kudryavtsev, K., Rumyantsev, V., Fadeev, M., Razova, A., Mikhailov, N., Shengurov, D., Gusev, S., Gusev, N., Morozov, S., “Mid-IR lasing in HgCdTe multiple quantum well edge-emitting ridges”, Applied Optics **62** (32), 8529-8534 (2023).

17. Razova, A. A., Fadeev, M. A., Rumyantsev, V. V., Utochkin, V. V., Dubinov, A. A., Aleshkin, V. Ya., Mikhailov, N. N., Dvoretsky, S. A., Gusev, N. S., Shengurov, D. V., Morozova, E. E., Gavrilenko, V. I., Morozov, S. V., “Whispering gallery mode HgCdTe laser

operating near 4 lm under Peltier cooling", Applied Physics Letters **123** (16), 161105-1-161105-5 (2023).

18. Rumyantsev, V. V., Mazhukina, K. A., Utochkin, V. V., Kudryavtsev, K. E., Dubinov, A. A., Aleshkin, V. Ya., Razova, A. A., Kuritsin, D. I., Fadeev, M. A., Antonov, A. V., Mikhailov, N. N., Dvoretsky, S. A., Gavrilenko, V. I., Teppe, F., Morozov, S.V., "Optically pumped stimulated emission in HgCdTe-based quantum wells: Toward continuous wave lasing in very long-wavelength infrared range", Applied Physics Letters **124** (16), 161111-1-161111-6 (2024).

19. Shao, J., Lu, W., Lü, X., Yue, F., Li, Z., Guo, S., Chu, J., "Modulated photoluminescence spectroscopy with a step-scan Fourier transform infrared spectrometer", Review of Scientific Instruments **77** (6), 063104 (2006).

20. Rayleigh, L., "The problem of the whispering gallery", Philosophical Magazine Series 6 **20** (120), 1001-1004 (1910).

21. Yang, Sh., Wang, Y., Sun, H., "Advances and Prospects for Whispering Gallery Mode Microcavities", Advanced Optical Materials **3** (9), 1136-1162 (2015).

22. Morozov, S. V., Rumyantsev, V. V., Zholudev, M. S., Dubinov, A. A., Aleshkin, V. Ya., Utochkin, V. V., Fadeev, M. A., Kudryavtsev, K. E., Mikhailov, N. N., Dvoretskii, S. A., Gavrilenko, V. I., Teppe, F., "Coherent Emission in the Vicinity of 10 THz due to Auger-Suppressed Recombination of Dirac Fermions in HgCdTe Quantum Wells", ACS Photonics **8** (12), 3526-3535 (2021).

23. Arias, J. M., Zandian, M., Zucca, R., Singh, J., "HgCdTe infrared diode lasers grown by MBE", Semiconductor Science and Technology **8** (1S), S255 (1993).

24. Hadji, E., Bleuse, J., Magnea, N., Pautrat, J. L., “Photopumped infrared vertical-cavity surface-emitting laser”, Applied Physics Letters **68** (18), 2480-2482 (1996).